Will be published:
Phys. Rev. A 73, 053603 (2006)

Quasi-condensate Growth on an Atom Chip

N.P. Proukakis[1*], J. Schmiedmayer[2] and H.T.C. Stoof[1]
[1] *Institute for Theoretical Physics, Utrecht University, Leuvenlaan 4, 3584 CE Utrecht, The Netherlands and*
[2] *Physikalisches Institut, Universität Heidelberg, 69120 Heidelberg, Germany*

We discuss and model an experiment to study quasi-condensate growth on an atom chip. In particular, we consider the addition of a deep dimple to the weak harmonic trap confining an ultracold one-dimensional atomic Bose gas, below or close to the characteristic temperature for quasi-condensate formation. The subsequent dynamics depends critically on both the initial conditions, and the form of the perturbing potential. In general, the dynamics features a combination of shock-wave propagation in the quasi-condensate, and quasi-condensate growth from the surrounding thermal cloud.

PACS numbers: 03.75.Kk, 05.30.Jp, 03.75.-b

I. INTRODUCTION

The recent achievement of effectively one-dimensional ultracold atomic samples on microfabricated surfaces, known as 'atom chips' [1] opens up the way for a number of applications, such as precision interferometric measurements [2, 3, 4, 5] and quantum computation [6, 7, 8]. One-dimensional (1D) geometries, in which the transverse confinement exceeds all other relevant energy scales in the system, offer improved atomic guidance and device miniaturization [9, 10]. This comes at the expense of increased phase fluctuations, which tend to destroy the coherence of the ensemble. Various equilibrium studies have already been performed both experimentally [11, 12, 13, 14] and theoretically [15, 16, 17, 18, 19, 20, 21, 22, 23, 24] to understand in particular this latter effect. However, a deeper understanding of the intrinsic dynamics of such systems is still lacking, including the issue of quasi-condensate formation, and the role of phase fluctuations on its growth dynamics. Although condensate formation has been studied in 3D geometries [25, 26, 27, 28, 29, 30], such studies are only now possible in 1D. In this paper, we discuss a realistic experiment which captures the dynamics of quasi-condensate formation and relaxation into a perturbed potential, by adding a dimple microtrap on an atom chip containing a gas of 1D ultracold Bose atoms.

The issue of quasi-condensate formation may be related to a recent 3D condensate growth experiment [27], which to date remains largely not understood. In particular, this experiment revealed, under conditions of slow cooling, an unexpected slow linear initial condensate growth. As these features were observed close to the transition point, the authors suggested this might be due to the enhanced phase fluctuations in this region, leading to the formation of a quasi-condensate that preceded the usual condensate growth. The dimensionality of our envisaged 1D experiment ensures the system remains in the regime of large phase fluctuations throughout its entire evolution. Moreover, under conditions of slow cooling from above the transition point, our results point towards a slow initial linear-like growth which is consistent with bosonic enhancement. However, a detailed comparison to the above experiment would require a full 3D calculation, and therefore lies beyond the scope of this paper.

The experimental scenario considered here is the following: An atom chip is first loaded with a certain number of atoms, at densities low enough to be in the 1D regime, and cooled to a prescribed low temperature. The approximately harmonic longitudinal confinement of the atoms is then perturbed by the addition of a deep dimple microtrap, of variable width, as shown in Fig. 1. Such a technique of local phase-space compression [31, 32] has been used to force a system of ^{23}Na atoms into the quantum-degenerate regime in a reversible manner in 3D [26]. A related approach has been used to create quantum-degenerate ^{133}Cs in 3D [33, 34], and in 2D [35]. In 1D, such a dimple can be created by optical and magnetic traps, although the optimum technique on an atom chip appears to be the application of electric fields to a separate electrode, as discussed in Appendix

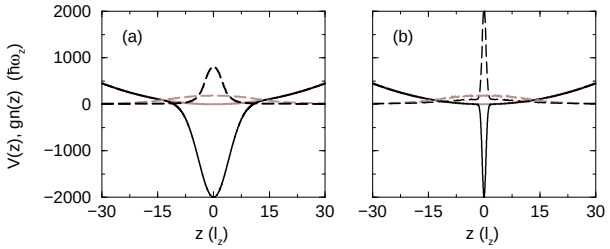

FIG. 1: Initial (brown lines) and final (black) longitudinal harmonic potentials (solid) and total densities (dashed) for a system of 2500 ^{87}Rb atoms at a temperature $T = 50nK$ for (a) a wide dimple $w = 4l_z$, and (b) a tight dimple $w = 0.5l_z$, with $z_D = 0$, $V_0 = -2000\hbar\omega_z$. Here, $l_z = \sqrt{\hbar/m\omega_z}$ is the longitudinal harmonic oscillator length.

*Present Address: School of Mathematics and Statistics, University of Newcastle, Merz Court, Newcastle NE1 7RU, United Kingdom

A. We study the resulting growth dynamics focusing on the regime of a very deep dimple, whose potential greatly exceeds all other energies in the system [36], as this leads to the most interesting non-equilibrium regime. If there is already a quasi-condensate present in the original trap, the addition of the dimple is found to lead to shock-wave formation and subsequent relaxation of the perturbed quasi-condensate in the dimple. In the opposite case of an initially incoherent ultracold atomic sample, we observe direct quasi-condensate growth from the surrounding thermal cloud. The nature of the dynamics additionally depends on the width of the dimple compared to the size of the atomic cloud, and on the dimple location. The distinct regimes of quasi-condensate dynamics can be probed by controlling the initial temperature, atom number and perturbing potential.

This paper is structured as follows: Sec. II discusses the methodology used to model the envisaged experiment. The dynamics following the addition of the dimple in the limit of low temperature is then discussed in Sec. III, paying particular attention to shock-wave formation (Sec. III A), its effect on the dynamics of the density at the trap centre (Sec. III B), and the effect of the width of the dimple compared to the size of the atomic cloud (Sec. III C). The effect of temperature is discussed in Sec. IV for both wide and tight dimples, with the latter case highlighting the interplay between spontaneous and stimulated growth in the dimple. Sec. V summarizes the examined regimes by means of a suitable graph, and Sec. VI features a brief summary. The discussion of experimental techniques which can be used to create the dimple trap on an atom chip has been deferred to Appendix A.

II. METHODOLOGY

To model the proposed experiment, we first prepare the desired initial state on the atom chip stochastically. This is achieved by means of the Langevin equation

$$i\hbar\frac{\partial\Phi(z,t)}{\partial t} = \left[-\frac{\hbar^2\nabla^2}{2m}+V_{\rm ext}(z)-\mu-iR(z,t) +g|\Phi(z,t)|^2\right]\Phi(z,t)+\eta(z,t)\,, \qquad (1)$$

describing the dynamics of the order parameter $\Phi(z,t)$ [37, 38, 39]. Here $V_{\rm ext}(z)=m\omega_z^2z^2/2$ denotes the longitudinal harmonic confinement, and $g=2\hbar a\omega_\perp$ is the one-dimensional coupling constant obtained by averaging over transverse gaussian wavefunctions, where a is the three-dimensional scattering length and $\omega_\perp$ the trap frequency in the transverse directions [40]. The chemical potential, μ, determines, for a given initial trap potential and temperature, the total atom number in the system. The atom chip trap is pumped from a thermal reservoir at a rate [37, 38, 39]

$$iR(z,t) = -\frac{\beta}{4}\hbar\Sigma^{\rm K}(z) \times\left(-\frac{\hbar^2\nabla^2}{2m}+V^{\rm ext}(z)-\mu+g|\Phi(z,t)|^2\right)\,. \qquad (2)$$

In accordance with the fluctuation-dissipation theorem, there is an associated gaussian noise contribution $\eta(z,t)$ obeying $\langle\eta^*(z,t)\eta(z',t')\rangle=(i\hbar^2/2)\Sigma^{\rm K}(z)\delta(z-z')\delta(t-t')$, where the brackets denote averaging over the realizations of the noise. The dependence of these quantities on the Keldysh self-energy $\hbar\Sigma^K(z)$ ensures that the trapped gas relaxes to the correct thermal equilibrium, as additionally verified by direct comparison to the modified Popov theory discussed elsewhere [16, 17, 18]. For simplicity, we choose in this work both the longitudinal and the transverse atom chip confinement to be harmonic, with respective trap frequencies $\omega_z=2\pi\times5$ Hz and $\omega_\perp=2\pi\times5000$ Hz, and present explicitly results for ^{87}Rb, with $a=5.32$nm. Unless otherwise specified, results will be given in dimensionless harmonic oscillator units of the original trap, such that lengths are scaled to the longitudinal harmonic oscillator length $l_z=\sqrt{\hbar/m\omega_z}$ and energies to $\hbar\omega_z$.

Once the system has fully relaxed to the desired equilibrium, we suddenly turn on a gaussian dimple potential and simultaneously remove the coupling to the heat bath. Switching off driving and dissipation terms, i.e., taking $R(z,t)=\eta(z,t)=0$, ensures that the total atom number on the atom chip remains fixed, as in the envisaged experiment, and thus only intrinsic dynamics of the system are taken into account. The dimple potential added is given by $V_D=V_0e^{-(z-z_D)^2/2w^2}$ where V_0 is the dimple depth, w its width, and z_D its location. A sudden introduction of the dimple potential is chosen, since this generates a highly non-equilibrium situation, which gives rise to the most interesting dynamics. For the chosen parameters, this corresponds to a trap turn-on timescale of 6μs, which is an experimentally realistic timescale. The subsequent analysis is based on averaging over many different initial realizations, which ensures that both density and phase fluctuations are accurately included. This is equivalent to averaging over a large number of independent experimental realizations with a variable initial phase, as typically done when investigating growth dynamics [25, 26, 27]. In our discussion, we assume the dimple is turned on at $t=0$.

III. LOW TEMPERATURE LIMIT

The sudden addition of a deep gaussian dimple on a harmonically confined pure condensate leads to a large atomic flux towards the center of the dimple, and thus to the development of a large local density gradient at symmetric points about the dimple centre, which, in turn, leads to the formation of two counter-propagating

shock wavefronts. The dynamics of the initial shock wave formation stage for a pure coherent condensate has been discussed under various related conditions in Refs. [41, 42, 43]. In addition, shock waves have already been observed experimentally in the context of rapid potential perturbations related to the formation of dark solitons [44] and vortex lattices [45]. In this paper, we discuss both short and long term dynamics in the dimple, and identify the distinct growth dynamics induced by the addition of the dimple. In particular, we highlight the competing effects of temperature, chemical potential and dimple width on these processes.

We start our analysis by considering the most general scenario of experimental relevance. The dimple of Fig. 1(a) is added onto a quasi-condensate with about $3,400$ atoms. This particular dimple has been chosen, as it can be easily generated with existing atom chips. A detailed discussion of how this can be achieved can be found in Appendix A.

In brief, we find the subsequent dynamics to be essentially controlled by two parameters: (i) Firstly, the dynamics depends critically on the amount of quasi-condensation present in the initial system. This is determined by the ratio of T/T_c, where T_c is the effective 1D 'transition' temperature. (ii) Secondly, the dynamics is sensitive to the relation of the spatial extent of the atomic cloud in the original trap compared to the effective width of the perturbing dimple potential.

A. Non-equilibrium Dynamics in the Dimple

For simplicity, we focus initially on the regime $T \ll T_c$, for which most of the atoms are in the quasi-condensate. Typical density snapshots of the growth dynamics in this limit are shown by the black lines in Figs. 2 (a)-(i). In our analysis, the 'transition' temperature T_c in the presence of interactions is determined numerically from our modified Popov theory [16, 17, 18, 19].

Once the dimple is turned on, the central density increases rapidly, until the instability towards shock-wave formation is reached [41, 42, 43]. The ensuing shock waves propagate towards the dimple edge and subsequently reflect back into the dimple centre. Individual profiles can be simulated by solving the Gross-Pitaevskii equation for a fully coherent condensate, yielding density profiles with large density variations, as shown by the green curves in the insets of Figs. 2(d)-(h). However, a detailed understanding of growth dynamics which enables a straightforward comparison to experiments requires the addition of random initial phases and subsequent averaging over such initial configurations. Such averaged profiles, obtained within our analysis, reveal the initial formation of a large central peak, followed by its break-up into two smaller peaks, moving in opposite directions towards the dimple edges, with the central peak re-emerging after a characteristic time determined by the dimple potential. The latter peak further splits into counter-propagating lower peaks, and so forth, until the gas equilibrates to the profile shown in Fig. 2(i). Such shock-wave dynamics would be largely suppressed if the dimple was much shallower, or if it were introduced on a much slower timescale.

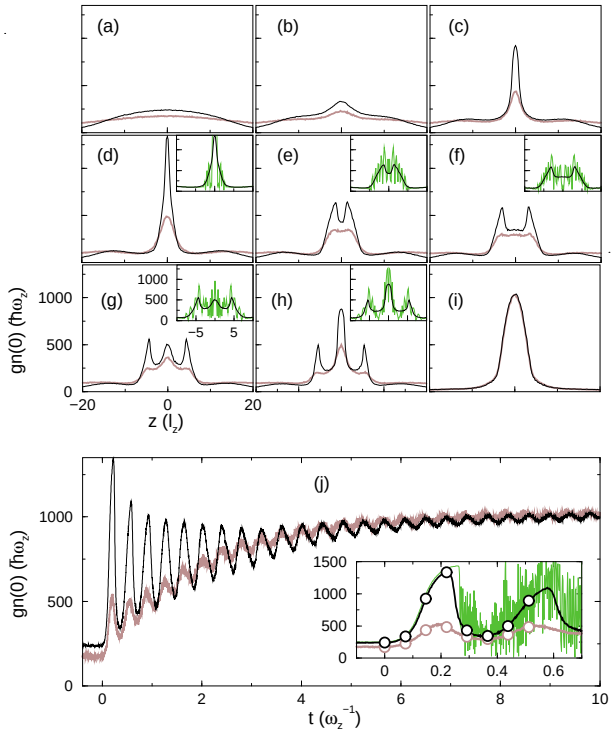

FIG. 2: (color online) Averaged snapshots of total density in the initial harmonic (a) and perturbed ((b)-(i)) trap, taken at equal time intervals, $\Delta t = 0.073\omega_z^{-1}$, for a gas of 3400 ^{87}Rb atoms. Profiles are shown at $T = 50$nK $\ll T_c$ (black lines) and $T = 200$nK $\approx T_c$ (brown). (i) Indistinguishable equilibrium profiles due to large dimple depth. Insets compare single-run results based on the Gross-Pitaevskii equation (green) to averaged stochastic profiles at $T = 50$nK. (j) Corresponding oscillations in averaged density at the trap centre. Inset highlights the first two oscillations, showing explicitly the times of the plotted snapshots (a)-(h), and comparing to results of Gross-Pitaevskii (green). Dimple parameters as in Fig. 1(a).

The long-term system dynamics is portrayed in the evolution of the central density of the gas shown by the black lines in Fig. 2(j). It features oscillations, on top of a growth curve. This complicated dynamics is a result of a number of competing processes occuring simultaneously. Firstly, the observed oscillations are a direct consequence of averaged shock-wave propagation in the quasi-condensate. In fact, the initial oscillatory dynamics in the low temperature limit resembles a suitably averaged single-run of the Gross-Pitaevskii equation, shown by the green lines in the inset to Fig. 2(j). The 'growth' part of the dynamics arises as a result of spatial compression of the trap, and features various contributions: In addition to quasi-condensate compression, there is an

additional process whereby all thermal atoms located in the dimple area fall into the perturbed trap by joining the quasi-condensate. This is ensured by the depth of the applied dimple, which largely exceeds all other relevant energies of the system. Moreover, thermal atoms located in the tails of the initial atomic cloud (as well as any quasi-condensate atoms located outside of the region of the dimple) are pulled into the trap centre, continuously interacting with the propagating quasi-condensate shock wave, and eventually leading to additional quasi-condensate growth. In the remaining part of the paper we discuss these competing processes in more detail by identifying suitable experimentally realistic limiting regimes.

B. Oscillation Frequencies

Firstly, we comment on the observed oscillations. The addition of the dimple corresponds essentially to an instantaneous local compression of the central region of the trap. For an easy visualization which captures the main dynamics discusssed here, let us consider the simplified case of a harmonic dimple of width comparable to the system size, such that essentially all of the dynamics is contained within a suitably defined 'dimple region'. In this case, the effect induced by the addition of the dimple is similar to that of an instantaneous increase in the harmonic frequency. This leads to excitation of the lowest compressional mode, which, for a pure condensate in the 1D mean field regime, has been predicted to occur at a frequency of $\sqrt{3}\omega_D$ [46, 47], as already observed experimentally [48], and additionally verified numerically in our simulations.

In the experimentally more realistic gaussian dimples considered here, we can define an effective harmonic frequency $\omega_D = \sqrt{V_0}/w$ at the central dimple region. Although the initial oscillation in the gaussian dimple occurs very close to the predicted frequency, the frequency shifts towards lower values, as soon as the quasi-condensate no longer feels a purely harmonic confinement, i.e., for system sizes larger than the effective dimple width. This shift becomes more pronounced in time as the quasi-condensate grows in the dimple. In addition, the observed oscillations are damped due to various effects. Firstly, unlike for a purely coherent system, the averaging performed over random initial phases in the presence of fluctuations leads to dissipation, precisely as would be the case in averaged condensate growth experiments in the presence of a non-negligible thermal cloud. Furthermore, the relative motion between the shock waves and the (mostly thermal) atoms entering the dimple region from the edges is expected to create an additional channel for dissipation. Finally, the addition of a gaussian dimple leads to excitations of multiple frequencies, which lead to beating effects and an accelerated decay of the oscillation amplitude.

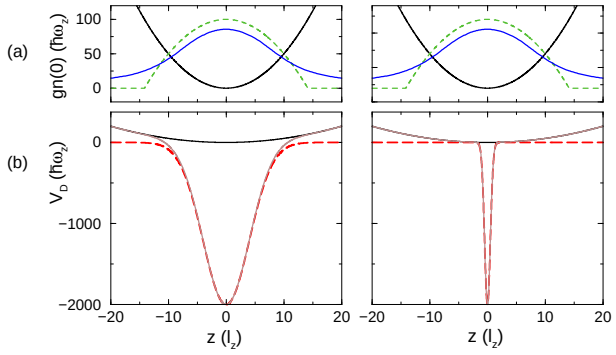

FIG. 3: (color online) (a) Initial density for a gas of $N \approx 960$ atoms at $T = 25$nK and $\mu = 100\hbar\omega_z$, such that $\mu/k_BT \approx 1$ (solid blue lines), versus corresponding zero-temperature Thomas-Fermi profiles (dashed green lines). The harmonic potential is also shown for easier visualization (solid black). (b) Initial (solid black) versus final (solid brown) potentials for the two dimples of Fig. 1. Corresponding dimple potentials V_D are shown by the dashed red lines.

C. Effect of Dimple Width

The above example featured a combination of shock-wave propagation and growth. These effects can be isolated by changing the form of the perturbation. Shock waves arise in the quasi-condensate already present prior to the addition of the dimple. On the other hand, the observed increase in the central density is the result of both local compression of the atoms in the dimple region, and of direct growth arising from (mainly thermal) atoms moving into the central region from the trap edge. As a result, oscillations dominate when the dimple width is comparable to the quasi-condensate system size, and for relatively small atom numbers, such that growth is minimized. On the other hand, the growth features are dominant in very tight traps for which the dimple width is much smaller than the system size.

These two contrasting regimes for the two opposite limits of wide and tight dimples, with respect to the effective system size, are shown in Fig. 3 for a reduced number of $N \approx 960$ atoms for computational convenience. To facilitate an easy comparison between these two limits we keep the dimple depth fixed. To give a simple visualization of this distinction, we note that, for the low temperature case considered here, the zero-temperature Thomas-Fermi profile (dashed green line in Fig. 3(a)) is a reasonable first approximation to the system density prior to the addition of the dimple (solid blue line). In the chosen harmonic oscillator units, the zero temperature Thomas-Fermi radius is defined by $R_{TF} = \sqrt{2\mu}$, where μ is the chemical potential of the system.

An effective dimple width, R_D can also be approximately defined as the point at which the dimple depth falls to 0.01 of its maximum value V_0, implying $R_D \approx 3w$. Fig. 3 plots both initial densities and potentials (top) and perturbed potentials (bottom) for the two opposite

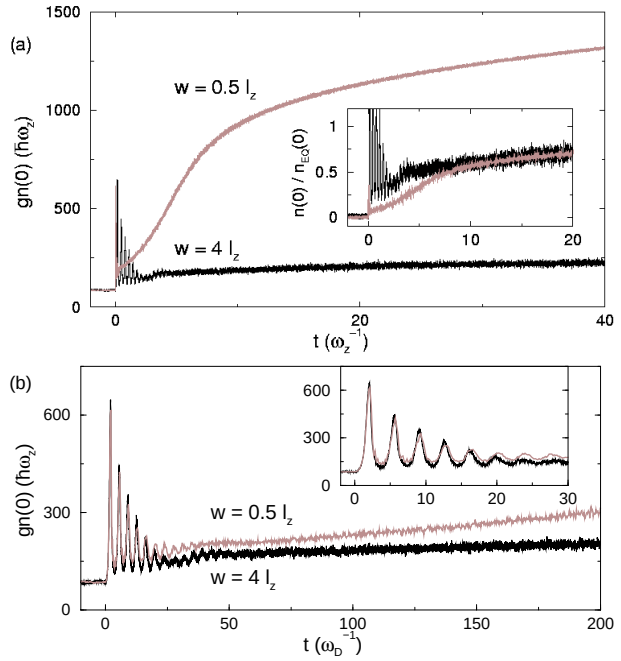

FIG. 4: (color online) (a)-(b) Dynamics of dimple central density for $N \approx 960$ atoms upon adding a broad dimple with $w = 4l_z$ (black) or a narrow one with $w = 0.5l_z$ (brown), as in Fig. 3. Time plotted in terms of (a) original trap timescale ω_z^{-1} and (b) dimple timescale ω_D^{-1}, with $\omega_D = 11.2\omega_z$ (black), or $89.4\omega_z$ (brown). Here $T = 25$nK and $\mu = 100\hbar\omega_z$, with $\mu/k_BT \approx 1$. Insets: (a) Same plot with densities approximately scaled to final equilibrium values $n_{EQ}(0)$, and (b) Initial regime highlighting the overlapping density oscillations.

regimes of $R_D \approx R_{TF}$ (left) and $R_D \ll R_{TF}$ (right). Note that the equilibrium densities in both dimple traps are essentially given by the Thomas-Fermi profiles in these traps. This is true for all atom numbers considered in this paper ($N < 3500$), for which the chosen large dimple depth ensures that all atoms can be accomodated within the central approximately harmonic dimple region (see also the density profiles in Fig. 1).

The system dynamics in these two opposite regimes is portrayed by the evolution of the central density in Fig. 4. This evolution is plotted both in terms of the original trap timescale ω_z^{-1} in Fig. 4(a), and in terms of the effective dimple timescale ω_D^{-1} in Fig. 4(b), as these reveal different dynamical features that we wish to comment on.

The actual relaxation timescale, and long-term dynamics in these opposing regimes are best compared when both curves are plotted in terms of the characteristic timescale ω_z^{-1} of the initial harmonic trap. Fig. 4(a) thus shows that the central density in the tight dimple increases much more significantly, due to the enhanced spatial compression. A comparison of the growth rate in the different dimple traps is facilitated in the inset to Fig. 4(a), by plotting the dynamics of the peak densities, approximately scaled to their respective equilibrium values. Although equilibration timescales appear to be comparable, the initial dynamics is slower in the tight trap, presumably due to the reduced overlap between the states in the initial and final traps.

The initial dynamics, including the shock-wave-induced oscillations are more appropriately investigated, when the same results are plotted in terms of the effective dimple timescale ω_D^{-1}, as in Fig. 4(b). This is because the oscillations are actually fixed by the frequency ω_D of the perturbed trap (multiplied by the factor of $\sqrt{3}$), which varies with dimple width w. When plotted in this manner, the initial dynamics feature a striking similarity in both amplitude and frequency of the respective central density oscillations, as shown in the inset. This is due to the fact that the initial dynamics is set by the quasi-condensate which is, in both cases, present over the entire extent of the dimple region. However, the subsequent growth is noticeably different, due to the enhanced compression in the tight dimple, leading to a much enhanced growth in the central density.

IV. EFFECT OF TEMPERATURE

All earlier discussion focused on the regime $T \ll T_c$. We now discuss the effect of changing the initial temperature of the system, with respect to T_c.

A. Wide Dimple

The density snapshots shown in Fig. 2 correspond to fairly 'typical' experimental regimes, for which $R_{TF}(0)$ is approximately equal to a few R_D, such that the addition of the dimple is accompanied by a combination of oscillations and growth. However, as the temperature of the initial sample increases towards T_c at fixed atom number, the propagating secondary density peaks in the averaged profiles become washed out, as shown by the brown lines in Fig. 2(a)-(h). This is due to the enhanced fluctuations in the initial state prior to the addition of the dimple. Nonetheless, the final averaged profile is almost independent of temperature, due to the large dimple depth, which overshadows all other energies of the system.

By comparing these two cases, we note that the amplitude of the initial oscillation is controlled by the ratio of the chemical potential μ to the thermal energy k_BT. Under conditions of strong condensation, such that $\mu/k_BT > 1$, the initial oscillation amplitude is large and can even exceed the equilibrium value. In the opposite regime, its amplitude is largely suppressed. In the limit of a sufficiently small atom number and a relatively broad dimple, the addition of the dimple perturbs the central density only mildly. Thus, the additional constraint of extremely low temperature ($k_BT \ll \mu$), leads essentially only to the appearance of oscillations without substantial growth.

B. Tight Dimple

The tight dimple, whose width is much smaller than the effective system size, creates a natural temporal separation between the initial shock-wave-induced oscillations and the subsequent growth dynamics. These competing effects exhibit different characteristics, depending on the ratio T/T_c, as shown in Fig. 5(a). This ratio can be controlled either by changing the temperature at constant total atom number, as discussed for Fig. 2 above, or by varying the atom number at fixed temperature. In this section, we choose to discuss the latter, as this enables a further distinction between spontaneous and stimulated bosonic growth. Note that, for the small atom numbers $400 < N < 1000$ considered here, the condition $R_{TF}(0) \gg R_D$ is always satisfied for the dimple with $w = 0.5l_z$.

Regarding the initial oscillations in the central density, we note that, as the atom number decreases, so does also the ratio of μ/k_BT determining the amplitude of the first oscillation. This leads to very strong suppresion when $\mu/k_BT \ll 1$, as shown by the bottom curve in the inset to Fig. 5(a). After quenching of these initial oscillations, we observe a 'secondary growth' dynamical phase. For small atom numbers, corresponding to large T/T_c, we observe a very slow initial growth in the central density. This will be shown to be consistent with spontaneous quasi-condensate growth from the thermal cloud. Increasing the atom number leads to a lower value of T/T_c, and to a significant quasi-condensate fraction in the initial trap, which yields a faster initial growth rate in the dimple.

To understand this in more detail, Fig. 5(b)-(c) plots the integrated quasi-condensate atom number in the dimple as a function of time for the cases (b) $T \approx T_c$, and (c) $T \ll T_c$. The quasi-condensate atom number is determined from a combination of local quadratic and quartic correlations of the order parameter $\Phi(z,t)$, as will be discussed in more detail elsewhere. The evolution is in both cases fitted by two distinct growth models, as in [25]. The first model includes both spontaneous and stimulated bosonic growth, and is fitted by dashed brown lines. It obeys

$$N_0(t) = N_0^{(i)} e^{\gamma t} \left[1 + \left(N_0^{(i)}/N_0^{(f)} \right)^{\delta} \left(e^{\delta\gamma t} - 1 \right) \right]^{-1/\delta} , \tag{3}$$

where N_0 the total quasi-condensate atom number in the dimple, the superscripts (i) and (f) denote respectively initial and final values, and γ corresponds to the initial growth rate. The value $\delta = 2/3$ assumes a growth rate linear in the difference of chemical potential of the thermal cloud and the quasi-condensate, for which $\mu \propto N_0^{2/3}$. The second model, fitted by the solid green lines, describes simple exponential relaxation to equilibrium via

$$N_0(t) = N_0^{(f)} \left(1 - e^{-\gamma t} \right) . \tag{4}$$

The limit $T \approx T_c$ shown in Fig. 5(b) is well described by the growth model of Eq. (3), indicating spontaneous and subsequent stimulated quasi-condensate growth in the dimple, analogous to the first condensate growth studies in 3D systems. Although the exponential relaxation model fails to describe the entire dynamics in this case, it nonetheless works well if fitted after a certain 'initiation' time [28]. In the opposite regime of $T \ll T_c$ shown in Fig. 5(c), the initial dimple dynamics is mainly governed by re-equilibration of the perturbed quasi-condensate in the combined trap. This obeys the exponential relaxation model well, indicating that the dynamics is dominated by stimulated growth.

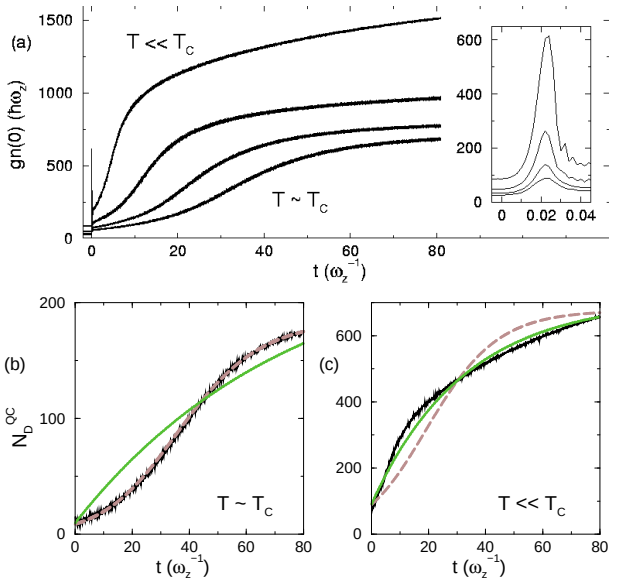

FIG. 5: (color online) (a) Central density dynamics in tight dimple ($w = 0.5l_z$) with increasing atom number (from bottom to top) $N \approx 420$, 490, 620 and 960, with $R_D \ll R_{TF}$ in all cases. The temperature is fixed to $T = 25nK$, and corresponding chemical potentials are $\mu/\hbar w_z = 5, 30, 60, 100$. Inset: Comparison of initial oscillatory dynamics. (b)-(c) Quasi-condensate growth in the dimple for (b) $N \approx 420$ ($T \approx T_c$), and (c) $N \approx 960$ ($T \ll T_c$). Each computed curve (black) is fitted with the growth curve of Eq. (3) (dashed brown), and the relaxation curve of Eq. (4) (solid green). The initial number of condensate atoms in the dimple is bigger in (c), due to the larger chemical potential.

The intermediate temperature regime features interesting, but complicated dynamics, as the effects of spontaneous and stimulated growth compete with each other. The above distinction between spontaneous and stimulated growth becomes less pronounced with increasing atom number, with the initial growth dynamics being well-modeled by an exponential relaxation curve even for the tight dimple considered here, when N is a few 1000 atoms.

V. SUMMARY OF DISTINCT REGIMES

The effect of adding a dimple trap to the centre of a weaker harmonic trap containing a 1D quasi-condensate was considered in the limit when the dimple depth greatly exceeds all other relevant energies in the system, i.e., $V_D \gg \mu, k_B T, \hbar\omega_z$. The presented analysis was restricted to the typical experimental regime satisfying the following length scale separation

$$l_\perp < \xi < (\lambda_{dB}, l_D) \ll l_z \ll (R_D, R_{TF}(0)) \qquad (5)$$

where $l_\perp = \sqrt{\hbar/m\omega_\perp}$ is the transverse harmonic oscillator length, $\xi = \hbar/\sqrt{4\mu m}$ is the healing length of the system, $\lambda_{dB} = \sqrt{2\pi\hbar^2/mk_BT}$ is the thermal de Broglie wavelength, $l_D = \sqrt{\hbar/m\omega_D}$ is the effective harmonic dimple oscillator length, $R_{TF}(0)$ is the zero-temperature Thomas-Fermi radius in the original harmonic trap, and R_D is the effective dimple width. Within this regime, the dynamics in the dimple displays an interesting interplay between shock-wave propagation in the perturbed quasi-condensate, and direct quasi-condensate growth.

The following important conclusions were reached about the accessible dynamical regimes in such systems:

- The initial dynamics for $T < T_c$ is dominated by shock-wave propagation, leading to large oscillations in the central density. The initial amplitude of such oscillations is controlled by the ratio of (μ/k_BT), yielding large oscillations when this is of order unity or larger.

- The long-term system dynamics is dominated by quasi-condensate compression and growth in the dimple, with this effect largely pronounced when the system size greatly exceeds the dimple width.

The different accessible regimes, along with the associated relevant parameters for (μ/k_BT) and $R_{TF}(0)/R_D$ are summarized by the evolution of the central density shown in Fig. 6. In this figure, each horizontal line (a)-(c) corresponds to a particular configuration of fixed initial atom number and dimple width. Left images (i) show the case $T \ll T_c$, while right images (ii) display the high-temperature limit $T \approx T_c$. The images shown portray, from top to bottom, the following cases:

(a) A relatively large atom number $N = 3400$, such that $R_{TF}(0)$ is slightly larger than R_D. This leads to noticeable growth, and additionally features pronounced and 'long-lived' oscillations when $\mu/k_BT \approx 1$.

(b) A sufficiently small atom number $N = 540$ and comparatively wide dimple, $R_{TF}(0) \approx R_D$, for which growth is suppressed and oscillations are the dominant feature in the low temperature limit.

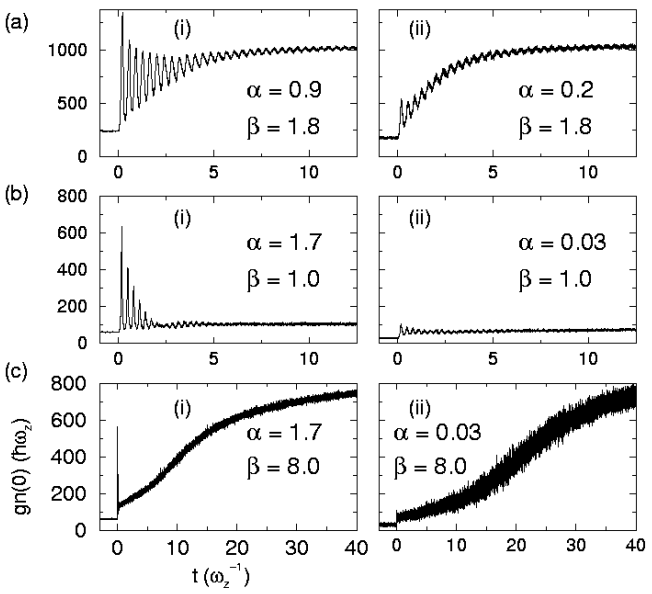

FIG. 6: Visualization of distinct regimes accessible in ultracold 1D Bose gases, upon addition of a deep dimple ($V_0 = -2000\hbar\omega_z$) at the centre of a weaker harmonic trap (i.e. $z_D = 0$), as manifested by the dynamics in the central density oscillations. From top to bottom, $N \approx$ (a) 3400, (b)-(c) 540, and $w =$ (a)-(b) $4l_z$, and (c) $0.5l_z$. Left images (i) correspond to $T \ll T_c$, with right images (ii) showing the opposite regime $T \approx T_c$. Each figure displays the corresponding approximate values of $\alpha = \mu/k_BT$, and $\beta = R_{TF}(0)/R_D$, determining the system dynamics.

(c) A very tight dimple $R_D \ll R_{TF}(0)$, featuring 'long-term' pronounced growth, after damping of any initial oscillations occuring. Note that the spontaneous bosonic growth contribution is pronounced here due to the small number of atoms.

Having identified the importance of the relation of the size of the atomic cloud compared to the dimple width, and of the chemical potential compared to the temperature of the system, we can now 'tailor' our experimental conditions to produce the desired dynamics.

Note that all dimples were considered to have the same depth, which exceeds all other relevant energy scales in the system. Thus, for the atom numbers considered here, the final densities are all described by Thomas-Fermi profiles in the dimple, and the dimple width is the relevant parameter determining the ensuing 1D dynamics.

The case of an off-centered dimple, with $z_0 \neq 0$, yields qualitatively similar behaviour, that will be discussed in more detail elsewhere. When the dimple falls within the initial quasi-condensate size, shock wave formation plays a key role in the subsequent dynamics. However, in the opposite limit of a dimple located outside of the quasi-condensate, the oscillations are largely suppressed, and quasi-condensate relaxation competes with quasi-condensate growth. The whole process is further modified by the asymmetry in the initial density distribution

with respect to the dimple centre, an effect which becomes particularly pronounced for shallow dimples.

VI. CONCLUSIONS

In conclusion, we studied one-dimensional quasi-condensate growth dynamics in a dimple microtrap created on top of the harmonic confinement of an atom chip. Rich novel dynamics were observed in the case of a deep dimple, whose depth exceeds all other energies of the system, displaying an interesting interplay between shock-wave propagation in the perturbed quasi-condensate, and direct quasi-condensate growth. The optimum observation of shock-wave dynamics, without the added significant growth of the central density, requires low temperatures $T \ll T_c$, a comparatively large chemical potential $\mu > k_B T$, and a dimple of width comparable to the system size. Understanding these processes in more detail is expected to contribute to fundamental issues in the dynamics of degenerate one-dimensional Bose gases, with potential applications in atom lasers and atom interferometers.

Acknowledgments

We acknowledge discussions with P. Krüger, S. Wildermuth, and in particular E. Haller. This work was supported by the Nederlandse Organisatie voor Wetenschaplijk Onderzoek (NWO), by the European Union, contract numbers IST-2001-38863 (*ACQP*), MRTN-CT-2003-505032 (*AtomChips*), HPRN-CT-2002-00304 (*FASTNet*), and the Deutsche Forschungsgemeinschaft, contract number SCHM 1599/1-1.

APPENDIX A: EXPERIMENTAL CREATION OF 1D DIMPLE POTENTIALS

This Appendix discusses various experimental techniques which can be used to create a dimple potential, in a quasi-1D atomic gas on an atom chip [1, 49, 50], in order to observe the dynamics discussed in this paper. The basic idea is to modify the 1D trapping potential with a small but localized attractive potential, which creates a tight potential minimum along the weak confining axis of the 1D trap.

To create the situation described in this paper one needs exceptionally smooth trapping potentials as obtained for example with atom chips nano-fabricated in gold layers on semiconductor substrates [10, 36, 51, 52]. On these atom chips, we can routinely create 1D traps with an aspect ratio of larger than 1000 [53]. The longitudinal confinement in the traps can be harmonic or box-like on the energy scale of the chemical potential, depending on the actual setup.

Starting from a 1D potential we can create a dimple on an atom chip by using (i) magnetic fields, (ii) electric fields and (iii) dipole potentials. In the following discussion of creating a dimple we neglect the longitudinal confinement of the original trap.

1. Creating the dimple with magnetic fields

On an atom chip, the 1D trap is formed in a magnetic minimum created by superimposing the magnetic field of a current in a straight wire by a homogeneous bias field [49, 51, 54, 55]. We assume the trapping wire to be parallel to the z-direction (Fig. 7) and the homogeneous bias field $B_{\rm bias} = (B_{\rm x}, B_{\rm y}, B_{\rm Ioffe})$ to be nearly orthogonal, i.e., $\mid B_{\rm Ioffe} \mid \ll \mid B_\perp \mid$ with $B_\perp = (B_{\rm x}, B_{\rm y}, 0)$. The component of the field along the wire direction, the Ioffe field $B_{\rm Ioffe}$, defines the minimum of the trapping field.

A dimple can be created by a second wire, located along the y-direction, and thus crossing the trapping wire (Fig. 7) [56]. A small current $j_{\rm D}$ in this *dimple*-wire creates a magnetic field which either *subtracts* from, or *adds* to, $B_{\rm Ioffe}$, thus creating a *dimple* or a *barrier* respectively. For a linear current crossing the trapping wire at $z = 0$, with the 1D trap at height h above it (Fig. 7 (a)), the dimple potential is given by

$$V_{\rm D}(z) = V_0 \frac{1}{1 + (z/h)^2} \, . \tag{A1}$$

The depth of the dimple potential $V_0 = g_F \mu_B m_F (\mu_0/2\pi)(j_{\rm D}/h)$ is determined by the magnitude of the magnetic field created by the current $j_{\rm D}$ at the position of the trap. Here μ_B is the Bohr magneton, g_F the Lande factor of the trapped atomic state $|F, m_F\rangle$ and $\mu_0 = 4\pi \; Gmm/A$ is the vacuum permeability. The longitudinal size (i.e. width) of the dimple is set by the distance h.

The geometry of the dimple depends on the ratio between h, the height of the trap above the dimple wire, and $d_{\rm trap}$, the distance of the atoms to the trapping wire:

$$\frac{\omega_\perp}{\omega_{\rm D}} \; = \; \frac{h}{d_{\rm trap}} \frac{\mid B_\perp \mid}{\sqrt{2 B_{\rm Ioffe} B_{\rm D}}} \tag{A2}$$

The parameters h and $d_{\rm trap}$ can be controlled independently, by either mounting the dimple wire above the trapping wire (Fig. 7(a)) or by rotating the trap towards the surface by rotating the bias field (Fig. 7(b)), thus yielding complete control of the dimple trap anisotropy. When the 1D gas is trapped relatively far from the trapping wire, the remaining residual disorder potentials [9, 10, 36] are reduced to a point where they are not visible even for tight transverse confinement of typical frequency $\omega_\perp \sim 2\pi(5$ kHz) [53, 57].

In a real experimental setup, the width of the wires and the exact form of the current distribution in the wires determines the potential. By measuring the magnetic dimple potential, as described in [9], we found that it is

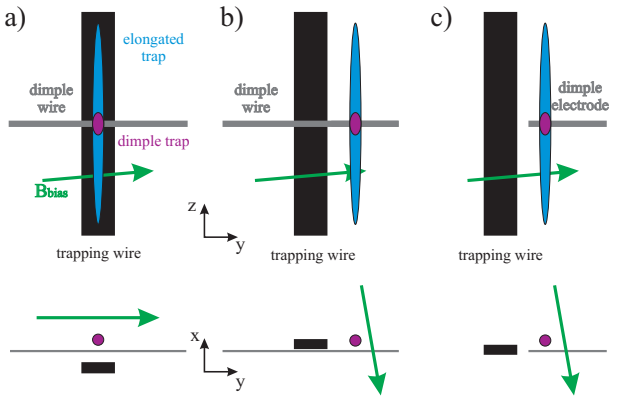

FIG. 7: (color online) Wire configurations for creating a dimple in a quasi-1D gas on an atom chip. (a) The dimple is created by the crossing wire placed above the trapping wire. The magnetic field created by the current flowing in the crossing dimple wire subtracts from the minimum of the 1D trap (Ioffe field $B_{\rm Ioffe}$). (b) By rotating the bias field the 1D trap is displaced and the dimple is created on the side of the trapping wire. To keep the trap symmetric around the dimple, a wire crossing is again required. (c) In the rotated geometry charging an electrode creates a strongly confining dimple, without the need for wire crossing.

actually very well described by a gaussian shape, as used in the calculations presented in this paper [57].

On an atom chip, a 1D trap with $\omega_\perp \sim 2\pi(5$ kHz) can be typically created by a 1000 mA current and a $B_\perp \sim 28G$. If the trap is then rotated towards the chip surface and positioned above an orthogonal wire at heights $h \sim (5-25)\mu$m, a current $j_{\rm D} \sim (10-100)\mu A$ in the dimple wire creates potentials like the ones described in the main part of this paper. The larger values of h correspond to wider dimples and require larger $j_{\rm D}$.

2. Creating the dimple by adding electric fields

A second way of implementing a controllable dimple on an atom chip is by using electric fields (Fig. 7(c)). An atom with electric polarizability α feels an attractive potential $V^{\rm el} = -\frac{1}{2}\alpha \mathbf{E}^2$. Charging up a wire positioned orthogonal underneath a trap will create a dimple potential [58].

In a simple model of a 1D trap at height h above the line charge Q, the electric dimple potential

$$V_{\rm D}^{\rm el}(z) = -\frac{1}{2}\alpha \frac{Q}{z^2+h^2} \qquad \text{(A3)}$$

has the same form as the magnetic dimple discussed above (Eq. (A1)). The ratio of the longitudinal to transverse confinement in the dimple depends again on the distance $d_{\rm trap}$ between the trapping wire and the atom trap, and on the height h above the line charge. This ratio can thus be adjusted over a broad range of values, by suitably choosing the position of the trap, as shown in Fig. 7(c).

Such a 1D electric dimple can be easily created on the atom chip with $\omega_\perp \sim 2\pi(5$ kHz) described above, once the trap is rotated towards the chip surface and positioned above an orthogonal wire. In the electric case, a few Volts of electric potential on the dimple wire create an adjustable dimple, whose parameters are similar to the ones described in this paper for typical trap heights of order $h \sim (5-25)\mu$m [57].

In a real setup one must again take into account the detailed geometry, the exact boundary conditions and the dielectric properties of the chip substrate. Measuring the potentials we found that they can be described, to good accuracy, by a gaussian shape [57].

Creating the dimple with electric fields has the advantage that a switchable dimple can be created even without the need for crossing the wires on the chip, as shown in figure 7(c). In addition, high resistivity materials can be used for charged structures, and this will dramatically reduce the thermal noise induced by Johnson noise currents [59, 60, 61, 62, 63, 64, 65, 66, 67], such that distances of 1 μm to the charged dimple wire are feasible.

3. Creating a dimple by superposing a dipole potential

A third way of creating a dimple on a atom chip is following [26] and superimposing a dipole potential on the atom chip trap [68]. The dimple is created by a tightly focused red-detuned laser beam. The size of the dimple is given by the focus size of the beam. The form of the dimple potential is gaussian, $V_{\rm D} = V_0\, e^{-(z-z_0)^2/2\sigma^2}$, and the size of the dimple is set by the numerical aperture of the imaging lens, and will typically be of order of 3-10 μm.

The dipole dimple can be created at arbitrary distance from the surface of the chip. It is the simplest way to create a tight dimple in cold atom experiments, and has been used in the condensate growth experiments at MIT [26], and the ^{133}Cs experiments at Innsbruck [33, 35]. In an atom chip environment, one has to take care of the stray light from the chip surface and the resulting interference structure inside the dimple. Scattered light will create speckles and form a additional disorder potential.

4. Switching the dimple

All three examples of dimple traps discussed above can be switched very fast. In the electric and magnetic cases, only very small currents or charges are needed, and rapid switching times ($\tau \ll 1\mu s$), much faster than the timescale of the transverse trapping frequency $\omega_\perp$, can easily be obtained. The same can be said for the dipole

dimple, for which the switching depends only on the light switching time, which can be again $\tau \ll 1\mu s$.

[1] C. Henkel, J. Schmiedmayer, and C. Westbrook, Eur. Phys. J. D **35** (2005) Special Issue - Atom Chips: manipulating atoms and molecules with microfabricated structures.

[2] E.A. Hinds, C.J. Vale, and M.G. Boshier, Phys. Rev. Lett. **86**, 1462 (2001).

[3] Y.-J. Wang, D.Z. Anderson, V.M. Bright, E.A. Cornell, Q. Diot, T. Kishimoto, M. Prentiss, R.A. Saravanan, S.R. Segal, and S. Wu, Phys. Rev. Lett. **94**, 090405 (2004).

[4] T. Schumm, S. Hofferberth, L.M. Andersson, S. Wildermuth, S. Groth, I. Bar-Joseph, J. Schmiedmayer, and P. Krüger, Nature Physics **1**, 57 (2005).

[5] Y. Shin, C. Sanner, G.-B. Jo, T.A. Pasquini, M. Saba, W. Ketterle, D.E. Pritchard, M. Vengalattore, and M. Prentiss, Phys. Rev. A **72**, 021604 (2005).

[6] T. Calarco, E.A. Hinds, D. Jaksch, J. Schmiedmayer, J.I. Cirac, and P. Zoller, Phys. Rev. A **61**, 022304 (2000).

[7] P. Treutlein, P. Hommelhoff, T. Steinmetz, T.W. Hänsch, and J. Reichel, Phys. Rev. Lett. **92**, 203005 (2004).

[8] M.A. Cirone, A. Negretti, T. Calarco, P. Krüger, and J. Schmiedmayer, Eur. Phys. J. D **35**, 165 (2005).

[9] S. Wildermuth, S. Hofferberth, I. Lesanovsky, E. Haller, M. Andersson, S. Groth, I. Bar-Joseph, R. Folman, and J. Schmiedmayer, Nature **435**, 440 (2005).

[10] P. Krüger, L.M. Andersson, S. Wildermuth, S. Hofferberth, E. Haller, S. Aigner, S. Groth, I. Bar-Joseph and J. Schmiedmayer, cond-mat/0504686.

[11] S. Dettmer, D. Hellweg, P. Ryytty, J.J. Arlt, W. Ertmer, K. Sengstock, D. S. Petrov, G. V. Shlyapnikov, H. Kreutzmann, L. Santos, and M. Lewenstein, Phys. Rev. Lett. **87**, 160406 (2001).

[12] I. Shvarchuck, Ch. Buggle, D.S. Petrov, K. Dieckmann, M. Zielonkowski, M. Kemmann, T.G. Tiecke, W. von Klitzing, G.V. Shlyapnikov, and J.T.M. Walraven, Phys. Rev. Lett. **89**, 270404 (2002).

[13] D. Hellweg, L. Cacciapuoti, M. Kottke, T. Schulte, K. Sengstock, W. Ertmer, and J.J. Arlt, Phys. Rev. Lett. **91**, 010406 (2003).

[14] S. Richard, F. Gerbier, J.H. Thywissen, M. Hugbart, P. Bouyer, and A. Aspect, Phys. Rev. Lett. **91**, 010405 (2003).

[15] D. S. Petrov, G.V. Shlyapnikov, and J.T.M. Walraven, Phys. Rev. Lett. **85**, 3745 (2000).

[16] J. O. Andersen, U. Al Khawaja, and H. T. C. Stoof, Phys. Rev. Lett **88**, 070407 (2002).

[17] U. Al Khawaja, J.O. Andersen, N.P. Proukakis, and H.T.C. Stoof, Phys. Rev. A **66**, 013615 (2002); *ibid.* **66**, 059902(E) (2002).

[18] U. Al Khawaja, N.P. Proukakis, J.O. Andersen, M.W.J. Romans, and H.T.C. Stoof, Phys. Rev. A **68**, 043603 (2003).

[19] N.P. Proukakis, Phys. Rev. A **73**, Vol. 1 (In Press, Jan. 2006) [cond-mat/0505039].

[20] D.L. Luxat and A. Griffin, Phys. Rev. A **67**, 043603 (2003).

[21] C. Mora and Y. Castin, Phys. Rev. A **67**, 053615 (2003).

[22] T.K. Ghosh, cond-mat/0402079.

[23] N.M. Bogoliubov, C. Malyshev, R.K. Bullough, and J. Timonen, Phys. Rev. A **69**, 023619 (2004).

[24] D. Kadio, M. Gajda and K. Rzazewski, Phys. Rev. A **72**, 013607 (2005).

[25] H.J. Miesner, D.M. Stamper-Kurn, M.R. Andrews, D.S. Durfee, S. Inouye, and W. Ketterle, Science **279**, 1005 (1998).

[26] D.M. Stamper-Kurn, H.J. Miesner, A.P. Chikkatur, S. Inouye, J. Stenger, and W. Ketterle, Phys. Rev. Lett. **81**, 2194 (1998).

[27] M Köhl, M.J. Davis, C.W. Gardiner, T.W. Hänsch, and T. Esslinger, Phys. Rev. Lett. **88**, 080402 (2002).

[28] M.J. Bijlsma, E. Zaremba, and H.T.C. Stoof, Phys. Rev. A **62**, 063609 (2000).

[29] C.W. Gardiner, M.D. Lee, R.J. Ballagh, M.J. Davis, and P. Zoller, Phys. Rev. Lett. **81**, 5266 (1998).

[30] M.J. Davis, S.A. Morgan, and K. Burnett, Phys. Rev. Lett. **87**, 160402 (2001).

[31] W. Ketterle and D.E. Pritchard, Phys. Rev. A **46**, 4051 (1992).

[32] P.W.H. Pinkse, A. Mosk, M. Weidemüller, M.W. Reynolds, T.W. Hijmans, and J.T.M. Walraven, Phys. Rev. Lett. **78**, 990 (1997).

[33] T. Weber, J. Herbig, M. Mark, H.-C. Nägerl, and R. Grimm, Science **299**, 232 (2003).

[34] Z.-Y. Ma, C.J. Foot, and S.L. Cornish, J. Phys. B **37**, 3187 (2004).

[35] M. Hammes, D. Rychtarik, B. Engeser, H.-C. Nägerl, and R. Grimm, Phys. Rev. Lett. **90**, 173001 (2003).

[36] P. Krüger, S. Hofferberth, E. Haller, S. Wildermuth, L.M. Anderrson, D. Gallego Garcia, S. Aigner, S. Groth, I. Bar-Joseph, and J. Schmiedmayer in L. Marcassa, C. Helmerson and V. Bagnato (eds.), Atomic Physics 19, AIP Conference Proceedings **770**, 144 (2005).

[37] H.T.C. Stoof, J. Low Temp. Phys. **114**, 11 (1999).

[38] H. T. C. Stoof and M.J. Bijlsma, J. Low Temp. Phys. **124**, 431 (2001).

[39] N.P. Proukakis, Las. Phys. **13**, 527 (2003).

[40] M. Olshanii, Phys. Rev. Lett. **81**, 938 (1998).

[41] B. Damski, Phys. Rev. A **69**, 043610 (2004).

[42] A.M. Kamchatnov, A. Gammal, and R.A. Kraenkel, Phys. Rev. A **69**, 063605 (2004).

[43] V.M. Perez, V.V. Konotop, and V.A. Brazhnyi, Phys. Rev. Lett. **92**, 220403 (2004).

[44] Z. Dutton, M. Budde, C. Slowe, and L.V. Hau, Science **293**, 663 (2001).

[45] T.P. Simula, P. Engels, I. Coddington, V. Schweikhard, E.A. Cornell, and R.J. Ballagh, Phys. Rev. Lett. **94**, 080404 (2005).

[46] S. Stringari, Phys. Rev. A **58**, 2385 (1998).

[47] C. Menotti and S. Stringari, Phys. Rev. A **66**, 043610 (2002).

[48] H. Moritz, T. Stöferle, M. Köhl, and T. Esslinger, Phys. Rev. Lett. **91**, 250402 (2003).

[49] R. Folman, P. Krüger, J. Schmiedmayer, J. Denschlag, and C. Henkel, Adv. At. Mol. Opt. Phys. **48**, 263 (2002).

[50] J. Reichel, Appl. Phys. B **74**, 469 (2002).

[51] R. Folman, P. Krüger, D. Cassettari, B. Hessmo, T. Maier, and J. Schmiedmayer, Phys. Rev. Lett. **84**, 4749

(2000).
[52] S. Groth, P. Krüger, S. Wildermuth, R. Folman, T. Fernholz, D. Mahalu, I. Bar-Joseph, and J. Schmiedmayer, Appl. Phys. Lett. **85**, 2980 (2004).
[53] S. Wildermuth, PhD. Thesis, Univ. Heidelberg (2005).
[54] J. Denschlag, D. Cassettari, and J. Schmiedmayer, Phys. Rev. Lett. **82**, 2014 (1999)
[55] J. Reichel, W. Hänsel, P. Hommelhoff, and T. W. Hänsch, Appl. Phys. B **72**, 81 (2001).
[56] With the fabrication method described in [52] we have recently also fabricated wire crossings at sub-μm scale in gold layers and semiconductors. (see: www.atomchip.org)
[57] E. Haller, Diplomarbeit, Univ. Heidelberg (2004).
[58] P. Krüger, X. Luo, M.W. Klein, K. Brugger, A. Haase, S. Wildermuth, S. Groth, I. Bar-Joseph, R. Folman, and J. Schmiedmayer, Phys. Rev. Lett. **91**, 233201 (2003).
[59] C. Henkel, S. Pötting, and M. Wilkens, Appl. Phys. B **69**, 379 (1999).
[60] C. Henkel, K. Joulain, R. Carminati, and J.-J. Greffet, Opt. Commun. **186**, 57 (2000).
[61] C. Henkel and S. Pötting, Appl. Phys. B **72**, 73 (2001);
[62] C. Henkel, P. Krüger, R. Folman, and J. Schmiedmayer, Appl. Phys. B **76**, 173 (2003).
[63] S. Scheel, P. K. Rekdal, P. L. Knight, and E. A. Hinds, Phys. Rev. A **72**, 042901 (2005).
[64] P. K. Rekdal, S. Scheel, P. L. Knight, and E. A. Hinds, Phys. Rev. A **70**, 013811 (2004).
[65] M. P. Jones, C. J. Vale, D. Sahagun, B. V. Hall, and E. A. Hinds, Phys. Rev. Lett. **91**, 080401 (2003).
[66] D. M. Harber, J. M. McGuirk, J. M. Obrecht, and E. A. Cornell, J. Low Temp. Phys. **133**, 229 (2003).
[67] Y.-J. Lin, I. Teper, C. Chin, and V. Vuletic Phys. Rev. Lett. **92**, 050404 (2004).
[68] D. Gallego, Diplomarbeit, Univ. Heidelberg (2005).